To be published in Applied Optics:

Title: Multiple shots averaging in Laser Flash measurement

Authors: Giovanni Ferrarini,Alessandro Bortolin,gianluca cadelano,lorenzo finesso,paolo bison

Accepted: 27 April 20

Posted 28 April 20

DOI: https://doi.org/10.1364/AO.389564

Multiple shots averaging in Laser Flash measurement

Giovanni Ferrarini,[1,*] Alessandro Bortolin,[1] Gianluca Cadelano,[2] Lorenzo Finesso,[3] and Paolo Bison[1]

[1]*ITC-CNR, Istituto per le Tecnologie della Costruzione, Consiglio Nazionale delle Ricerche, Corso Stati Uniti 4, 35127, Padova, Italy*
[2]*ISAC-CNR, Istituto di Scienze dell'Atmosfera e del Clima, Consiglio Nazionale delle Ricerche, Corso Stati Uniti 4, 35127, Padova, Italy*
[3]*IEIIT-CNR, Istituto di Elettronica e di Ingegneria dell'Informazione e delle Telecomunicazioni, Consiglio Nazionale delle Ricerche, Via Gradenigo 6/B, 35131, Padova, Italy*
**giovanni.ferrarini@itc.cnr.it*

Abstract: The laser flash method is a well-known procedure to determine the thermal diffusivity of a wide range of materials. However, in some cases there is the need of limiting the input power, or measuring materials with high thermal capacity, or investigating thick samples. These conditions lead to a reduction of the signal-to-noise ratio. Therefore, we propose a new laser flash control and data acquisition system, that is able to repeat multiple times the emission of the laser impulse and the measurement of the thermal response of the specimen. With the average of several measurements, it is possible to obtain a decrease of the noise when working with low power inputs.

1. Introduction

The nondestructive evaluation of materials is a fundamental tool for the industrial production, as it can significantly contribute to improve the design of the components and to the assessment of the production quality [1,2]. Several methods and techniques are available to analyze material samples and investigate the chemical, structural, or thermal properties [3]. The latter are important, for example during the design phase of a component. The thermal properties are used as input of simulation models [4] and providing accurate data to the models is the basic condition to obtain reliable predictions. A predetermined value of a thermal property could be also the desired requirement of an industrial component. The measurement on a component coming from different production batches could help the manufacturer to identify anomalous products [5]. Broadly speaking, the use of a nondestructive method is a great advantage, especially when dealing with real-size mockups [6] or when performing on-site evaluations [7].

Among all available methods for determining the thermal properties [8], one of the most popular is the Laser Flash Method (LFM) [9]. In the standard LFM procedure where a heat flux is applied on the front face of a specimen and the temperature is measured on the back of the specimen [10–12]. Single-side configurations are available [13]. The LFM is typically applied to small size disk-shaped specimens in order to measure their thermal diffusivity (α value). The main advantages of the method are its simplicity, speed of measurement, and the possibility to measure the thermal diffusivity of a large variety of materials within a wide temperature range. The LFM is chosen also because it gives the possibility of measuring the thermal conductivity. To this end a procedure with adequate reference samples must be set up. In alternative, knowledge of the density (ρ), that can be measured through Archimedes principle, and of the specific heat (c_p), that can be obtained through differential scanning calorimetry (DSC), makes it possible to derive the thermal conductivity as the product of the density (ρ), the specific heat (c_p), and the thermal diffusivity (α) [14].

The original LFM has been widely studied and applied, expecially for the characterization of thermal barrier coatings (TBC) [15–18]. Several modifications have been proposed, both from the mathematical [19] and from the experimental standpoint [20,21] to improve the results and quantify the possibilities and limitations of the method. One critical issue is limiting the input power, that for some ranges of thermal properties and thickness of the specimen may lead to an unwanted and nonuniform overheating [17]. Vozàr and Hohenauer [22] proposed to divide the energy of a single laser pulse into smaller repeated pulses, obtaining results comparable to the traditional technique. Recently, Ruffio et al. [23] explored the use of a high speed laser pulse train in order to improve the signal-to-noise ratio (SNR). This study proposes a novel experimental setup that allows the automatic repetition of single pulses with a user defined time delay between each pulse. This leads to an increase of the SNR, as shown in the following sections. This allows to use the LFM method with lower input power on specimens that have an unfavorable combination of thermal properties and thickness.

2. Thermal diffusivity measurement – Laser Flash Method

2.1 Mathematical model

Several mathematical models are available to describe the heat conduction problem of this method. Considering the specimen under analysis as a slab of thickness *l*[m], the heating pulse can be modeled as a Dirac delta function *δ(t)*. The heating is uniformly distributed over the slab surface and produces a one dimensional thermal diffusion through the thickness of the specimen. The heat transfer problem is described by Eq. (1):

$$u_{zz} - \frac{1}{\alpha} u_t = 0 \tag{1}$$

where $u=u(z,t)$ is the function describing the temperature in the body, that depends on the space coordinate z and time t[s], and α is the thermal diffusivity [$m^2\ s^{-1}$]. It is possible to choose two different hypotheses: the adiabatic case and the non-adiabatic case.

Under the adiabatic hypothesis, the exchange with the environment (h is the heat exchange coefficient [$W\ m^{-2}\ K^{-1}$]) is neglected, as shown in Fig. 1.

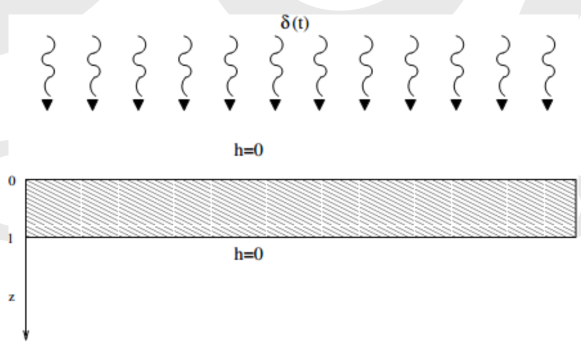

Fig. 1. Scheme of the thermal problem: the adiabatic case. The heating pulse is modeled as a Dirac delta function *δ(t)* and produces a one dimensional thermal diffusion through the thickness of the specimen. Under the adiabatic hypothesis, the exchange with the environment is neglected.

The boundary conditions are:

$$\begin{gathered} -\lambda u_z(0,t) = Q \cdot \delta(t) \\ u_z(l,t) = 0 \end{gathered} \tag{2}$$

where λ is the thermal conductivity [$W\ m^{-1}\ K^{-1}$], *δ(t)* is the Dirac delta function and Q the strength of the pulse [J]. The initial condition is:

$$u(z,0) = 0 \quad (3)$$

Solving through the application of the Laplace Transform, it is possible to obtain the temperature evolution in time for each point of the slab, as described in Eq. (4):

$$u(z,t) = \frac{Q}{\lambda}\frac{\alpha}{l}\left[1 + 2\sum_{n=1}^{\infty}(-1)^n e^{-n^2\pi^2\frac{\alpha}{l^2}t}\cos\frac{n\pi}{l}(z-l)\right] \quad (4)$$

that may be rewritten also in the form of Eq. (5):

$$u(z,t) = \frac{Q}{\epsilon\sqrt{\pi t}}e^{-\frac{z^2}{4\alpha t}}\left[1 + 2\sum_{n=1}^{\infty}e^{-\frac{(2nl)^2}{4\alpha t}}\cosh\frac{4nzl}{4\alpha t}\right] \quad (5)$$

In Eq. (5), ε is the thermal effusivity [J K^{-1} m^{-2} s$^{-1/2}$], defined as in Eq. (6):

$$\epsilon = \sqrt{\lambda\rho c_p} \quad (6)$$

where ρ is the density [kg m^{-3}] and c_p is the specific heat [J kg^{-1} K^{-1}] of the material. It is worth noting that Eq. (4) represents the deviations from the solution at the end of the process, that is the behavior of *u(z,t) when* $t \rightarrow \infty$*,* while Eq. (5) represents the deviations from the behavior of the semi-infinite body, that is *u(z,t)* when $t \rightarrow 0$. Defining the Fourier number *Fo* as in Eq. (7):

$$Fo = \frac{\alpha t}{l^2} \quad (7)$$

it is possible to represent the results of Eq. (4), setting the value of the leftmost parameter group *(Qα/λl)* equal to 1. This is done in Fig. 2, where the *x*-axis is the normalized thickness *(z/l)* of the slab and the *y*-axis is the ratio between the temperature *T* and the T_{inf} temperature for $t \rightarrow \infty$.

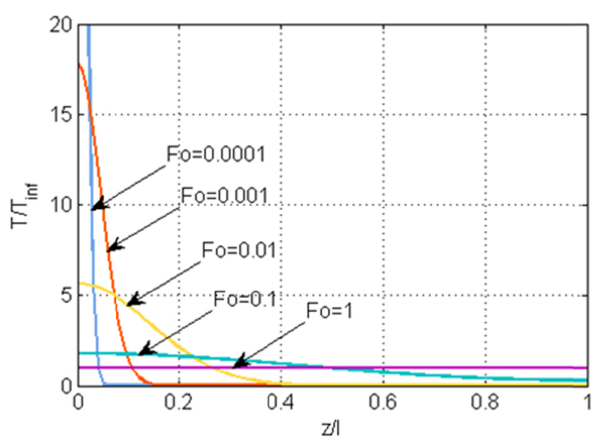

Fig. 2. Representation of Eq. (4) for increasing values of the Fourier number *Fo*. The value of the parameter group (*Qα/λl*) is equal to 1, the *x*-axis is the normalized thickness (*z/l*) of the slab. A significant temperature increase may occur on a part of the specimen and may lead to undesired effects.

The diagram shows that a significant temperature increase may occur on a part of the specimen and may lead to undesired effects. For example, materials such as Zirconium oxides or Yttrium oxide partially stabilized Zirconium (YPSZ), that have low thermal effusivity values with respect to metals, show a temperature increase on their front faces up to four times higher than a metal (e.g. an AISI304 austenitic steel) [15]. Furthermore, the heat pulse may create a high temperature gradient inside the specimen due to the low thermal diffusivity of YPSZ. The combined effect of high temperature increase and temperature gradient within the sample may lead, for certain values of the toughness of the specimen, to microstructural modifications of the sample itself such as growing or reopening of microcracks [15]. A high temperature gradient may also introduce some errors in the measurement of thermal properties with a strong temperature dependence. A high temperature increase leads also to a non-negligible heat exchange with the environment.

The non-adiabatic model of the Laser Flash method, sketched in Fig. 3, is always based on Eq. (1) where boundary conditions of Eq. (8) are chosen, and a pulse of finite duration t_h is considered:

$$-\lambda u_z(0,t) = Q \cdot [H(t) - H(t-t_h)] - hu(0,t)$$
$$u_z(l,t) = 0 \qquad (8)$$

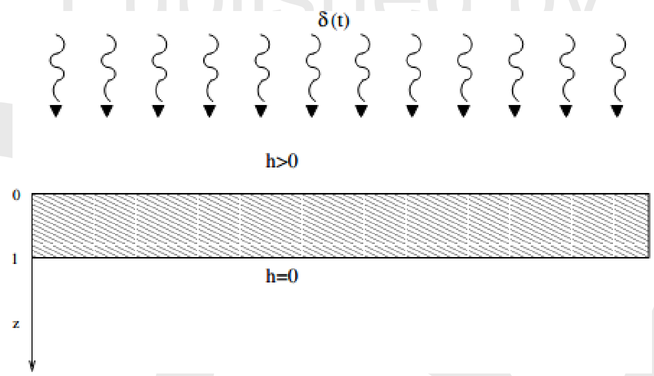

Fig. 3. Sketch of the thermal problem with exchange with the environment on the heated side. In this case, the heat exchange with the environment on the heated side of the specimen is described by the Newton linear law.

where *H(t)* is the Heaviside step function and *h* is the heat exchange coefficient. The heat exchange with the environment on the heated side of the specimen is described by the Newton linear law (fixed heat exchange coefficient and reference ambient temperature). Under this assumption, the temperature profile over time on the back face of the specimen is given by Eq. (9):

$$T(t) = \frac{Q}{h}\sum_{i=1}^{\infty}\frac{2\sin(\mu_i)}{\mu_i + \sin(\mu_i)\cos(\mu_i)}\left[\exp\left(-\mu_i^2\frac{\alpha}{l^2}(t-t_h)\right) - \exp\left(\mu_i^2\frac{\alpha}{l^2}t\right)\right] \qquad (9)$$

where μ_i is the *i*-th positive root of the transcendental Eq. (10):

$$\mu\tan(\mu) = B \qquad (10)$$

B is the Biot number, defined by the Eq. (11):

$$B = \frac{hl}{\lambda} \qquad (11)$$

The model described by Eq. (9) depends both on known and unknown parameters. The two known parameters are the sampling rate of the acquisition board, determining the times *t* of the temperature acquisition, and the pulse duration t_h that is set by the heating source (laser equipment).

2.2 Data analysis

To gain a better understanding of the data analysis procedure we introduce an abstract model. Let us consider n observations (y_i, x_i), $i=1,\dots,n$, where the dependent variables (measurements) $y_i \in \mathbb{R}$ are related to the independent variables (regressors) $x_i \in \mathbb{R}^m$ via a (generally) nonlinear relationship $y_i = g(x_i, \theta^*) + \varepsilon_i$, where ε_i is an unobserved noise. The functional relationship $g()$ is known modulo the components of the vector $\theta^* \in \mathbb{R}^p$, which are fixed but unknown parameters, to be estimated on the basis of the observations. The correspondences between the abstract formulation and Eq. (9) are as follows, $x_i = t_i$ is the i-th sampling time, $y_i = T(t_i) + \varepsilon_i$, and $\theta^* \in \mathbb{R}^3$ with:

$$(\theta_1^*, \theta_2^*, \theta_3^*)^T = \left(\frac{Q}{h}, \frac{\alpha}{l^2}, B\right)^T \tag{12}$$

Define $\boldsymbol{y} = (y_1,\dots,y_n)^T$, $g_i(\theta) = g_i(x_i,\theta)$, $\boldsymbol{g}(\theta) = (g_1(\theta),\dots,g_n(\theta))^T$, where $\theta^* \in \mathbb{R}^p$, and $S(\theta) = ||\boldsymbol{y} - \boldsymbol{g}(\theta)||^2 = \sum_{i=1}^{n}\left(y_i - g_i(\theta)\right)^2$, the function of θ measuring the goodness of fit of model $\boldsymbol{g}(\theta)$ to the measurements $\boldsymbol{y}$. The least squares estimator $\hat{\theta}$ of the parameter θ^* is defined as the minimizer $\hat{\theta} \coloneqq argmin_\theta S(\theta)$. Imposing the first order conditions for the minimum one gets the Eq. (13):

$$\frac{\partial}{\partial \theta_j} S(\theta) = 2\sum_{i=1}^{n}\left(y_i - g_i(\theta)\right)\frac{\partial}{\partial \theta_j} g_i(\theta) = 0 \tag{13}$$

which, letting $G = ||\frac{\partial}{\partial \theta_j} g_i(\theta)||_{ij} \in \mathbb{R}^{p \times p}$, can be written in matrix form as (normal equations) Eq. (14):

$$G^T\left(\boldsymbol{y} - \boldsymbol{g}(\theta)\right) = 0 \tag{14}$$

These equations in θ do not have a closed form solution and iterative schemes need to be setup to find $\hat{\theta}$. On the other hand the solution is straightforward in the linear case, i.e. when $\boldsymbol{g}(\theta) = X\theta$ for some $X \in \mathbb{R}^{p \times n}$, and it is worth deriving it as it sheds light on the general case. In the linear case one trivially gets $G = X$, thus the normal equations are $X^T(\boldsymbol{y} - X\theta) = 0$ and their solution is $\hat{\theta} = (X^TX)^{-1}X^T\boldsymbol{y}$. In case of repeated observations $\boldsymbol{y}_t$, $t=1,\dots,N$, where each $\boldsymbol{y}_t \in \mathbb{R}^n$, there are two equivalent ways of computing the estimator. In the first way one starts computing the N estimators, $\hat{\theta} = (X^TX)^{-1}X^T\boldsymbol{y}_t$, for $t=1,\dots,N$, and then computes their average $\hat{\theta}_A \coloneqq \frac{1}{N}\sum_{t=1}^{N}\hat{\theta}$. Alternatively, one starts computing the averaged observations $\overline{\boldsymbol{y}} \coloneqq \frac{1}{N}\sum_{t=1}^{N}\boldsymbol{y}_t$ and then computes the estimator $\hat{\theta}_B = (X^TX)^{-1}X^T\overline{\boldsymbol{y}}$. By inspection of the above formulas it is immediate to verify that $\hat{\theta}_A = \hat{\theta}_B$. The advantage of the N repeated observations is to reduce the variance of the estimator by a factor $1/N$. In the nonlinear case the two procedures for dealing with repeated observations are not equivalent. On the other hand when (as is usually the case) the estimators are consistent, i.e. $\hat{\theta} \rightarrow \theta^*$ for $n \rightarrow \infty$, since in a neighborhood of θ^* the nonlinear model is well approximated with its linearized version $g(\theta) \approx g(\theta^*) + G(\theta - \theta^*)$, the equivalence of the two procedures for repeated observations still holds.

A good reference for this section is Seber [24], to which the interested reader is referred for the missing mathematical details.

2.3 Experimental layout

The laser flash apparatus allows the execution of different types of experiments. In the basic configuration the bell jar is lifted and the experiment is performed at room temperature and atmospheric pressure. Including in the setup the bell jar, it is possible to perform experiments in a controlled environment (flowing gas such as Nitrogen or Argon) or in vacuum, up to 10^{-6} Torr. Another option is including a furnace, that could drive the specimen up to 1600 °C. Fig. 4 shows the experimental layout including the main elements.

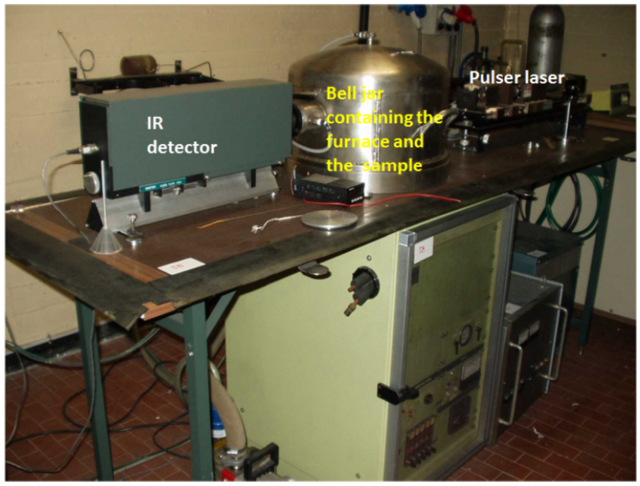

Fig. 4. The experimental layout consists (from right to left) in a laser, a bell jar containing the furnace and the sample holder, and an infrared detector. The data acquisition system is placed on the back side of the apparatus.

The experimental layout includes six elements: a laser, a sample holder, a bell jar, a furnace, a detector, and a control and data acquisition system. The laser is a Nd doped YAG solid state laser (wavelength 1064 nm) pumped by two xenon filled flash lamps. The power supply is capable of rep-rates of over 600 pulses per minute with the output energy continuously adjustable from the lasing threshold to at least 30 joules by varying the flash lamp voltage and the lamp pulse width. The lamp voltage is adjustable from 0 to 1000 volts. The pulse width is adjustable from 10 microseconds to 2 milliseconds. The sample holder is a graphite and molybdenum ring, and is placed inside a bell jar. The bell jar has two infrared transparent windows and is connected to a dual stage vacuum system and to a gas flowing circuitry. The bell jar could also host a furnace, that consists in a tantalum foil and is monitored by a Platinum-Rhodium Thermocouple. The detector is a Teledyne J10D (InSb, range 2-5.5 μm) operating in photovoltaic mode and connected to a P9 transimpedance amplifier.

Before the experiments, the samples may be painted with a high emissivity black varnish (Kontakt Chemie Graphit 33) to improve the thermal detector measurement and the absorption of the laser pulse on the opposite side respectively.

3. The novel experimental setup

The existing Laser Flash setup has been modified introducing a new hardware and software setup. In particular, the data acquisition system and the experiment control system have been changed. The underlying idea is making possible the repetition of multiple measurements on the same sample.

The architecture of the system is shown in Fig. 5a and includes: a computer with dedicated software, an analog input/digital output controller, a laser controller, a laser, an infrared sensor. In Fig. 5a the base architecture is represented on the right column, where the laser controller activates the laser heating the specimen. The temperature variation is detected by an Infrared sensor. The improved architecture is based on an analog input/digital output controller, realized with a National Instrument NI 6211 module. This device has a 16-bit analog input (sampling up to 250 kS/s) with an adjustable input range up to ±10V. The device has an internal base clock up to 80 MHz and a digital output (TTL 5V). The device has been connected on its analog input channel to the infrared detector (described in the next section) and on its digital output channel to the laser controller.

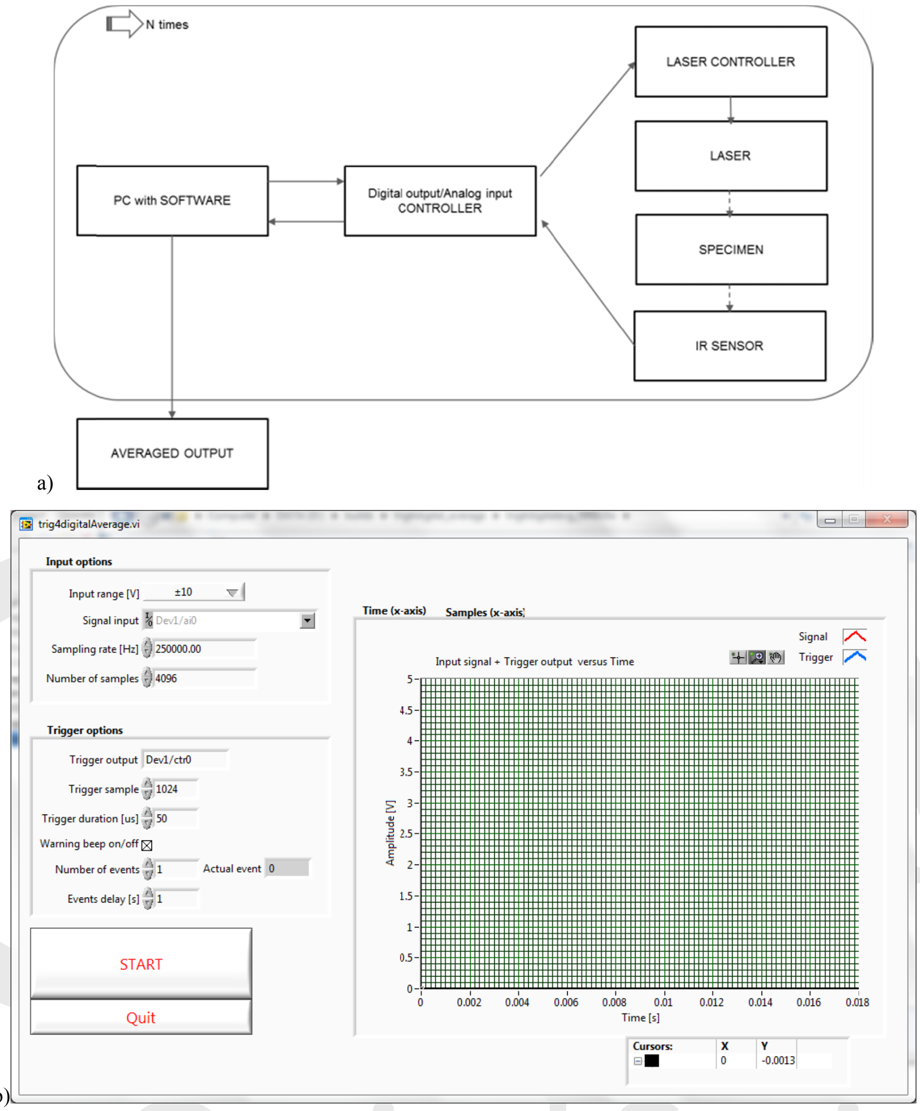

Fig. 5. a) Block diagram of the measurement setup. It includes the hardware architecture, as shown in Fig. 4, and the measurement procedure where a single laser shot is repeated N times to obtain the averaged output. b) Screenshot of the user interface of the developed software, showing the measurement variables available for the user.

A new software developed in Labview has been created for the measuring process. The user interface is shown in Fig. 5b. The software relies on the Daqmx SubVIs, that manages the input and output channels of the data acquisition board. The user can choose the input range and the sampling rate, that is adjusted on the estimated signal coming from the detector. The buffer size is chosen to maximize the timing accuracy of the board. The user can also choose when the laser shot is performed and the duration of the shot. Another important feature for the user is the possibility of repeating the measurement, choosing also the delay between repetitions. At the end of the repetitions, the user obtains the data of all the repetitions and the average value.

The number of repetitions and the delay between each repetition should be chosen taking into account both the kind of material under test and the experimental conditions (specimen temperature, environment). Following the model described in section 2, the user could predict the specimen behavior and assess the measurement uncertainty related to the temperature of the specimen [21].A first test of the hardware and software has been made short-circuiting the input and the output of the board. The second testing round has been a long set of measurements on a sample with the possibility of detecting also the laser signal. This has allowed the quantification of a repeatable delay between the output from the control board and the actual laser shot.

4. Materials and methods

The two types of tested specimens are part of an ongoing research on thermal barrier coatings: the first is made of AISI 304 stainless steel, that is chosen as a reference for the apparatus testing, while the second is made of Zirconium oxide. The Zirconium oxide (ZrO_2) specimen has been thermally treated in an oven at 1100 °C for 300 hours to simulate the aging of the material under working conditions. The series of measurements are listed in Tab. 1. The number of repetitions is chosen to increase of a desired quantity the SNR.

Table 1. List of measurements

Series	Sample	Environment	Number of repetitions
#1	AISI 304	Room temperature	100
#2	ZrO_2	Room temperature	16
#3	ZrO_2	Room temperature, vacuum	16
#4	ZrO_2	High temperature (1100°C)	16

The AISI 304 sample has a thickness of 1.024 mm, while the Zirconium oxide sample thickness is under measurement in the project. Therefore, in this paper the results for AISI 304 are listed as thermal diffusivity, while the results for Zirconium oxide are expressed as the output of the fitting parameter α/l^2.

For each series, two averaging methods are performed and compared. Firstly, the data of the average have been fitted with a nonlinear solver (implementing the Levenberg-Marquardt algorithm) available in the Matlab environment. Then the obtained parameters have been used as the starting point for the fitting of each repeated measurement. The saving in computational time is remarkable when performing the fit of the averaged value with respect to fitting each measure and successively averaging the parameters. This is due to two reasons that have a different effect on the calculation. The first is that the fitting process is the most time-consuming calculation, therefore removing the need of repeating it decreases the time proportionally to the number of repetitions. The second reason is that the speed of the fit typically decreases, going from up to a minute to just few seconds on the same computing machine (MacBook Pro with 2.6 GHz dual-core intel i5 and 8 GB RAM), when the data have a low SNR. Therefore, the fit of any single measurements (one shot) is more time consuming than the fit of the average shot.

For each fit, the root mean square of the differences between the experimental data and the fit is chosen as an indicator of the measurement noise [16]. Then the SNR is defined as the ratio between the maximum value of the fitted signal and the aforementioned noise.

5. Results

The results for the AISI 304 specimen are shown in Tab. 2, where it is possible to note that the two averaging processes described above lead to the same value of thermal diffusivity, a result that is compatible with the literature references [17].

Table 2. Results for the measurement series #1 on AISI 304. *single fit

Series and Method	Estimated parameter α/l^2 [s^{-1}]	Thermal diffusivity [$m^2\ s^{-1}$]	Standard deviation of the fitting error [a.u.]	Signal-to-noise ratio [a.u.]
#1 AISI 304 Fit on the average value	3.96	$4.1 \cdot 10^{-6}$	$5.4 \cdot 10^{-5}$	24.2
#1 AISI 304 Average of the fits on each repetition	3.96	$4.1 \cdot 10^{-6}$	$4.8 \cdot 10^{-4}$*	2.7*

The noise level on a single measurement is, as expected, higher than the averaged value, theoretically by a factor equal to the square root of the number of measurements. A better comparison of the noise level is proposed in Fig. 6, where the fit on the average value (average shot) and the fit on a single measurement (single shot) are plotted against the experimental data.

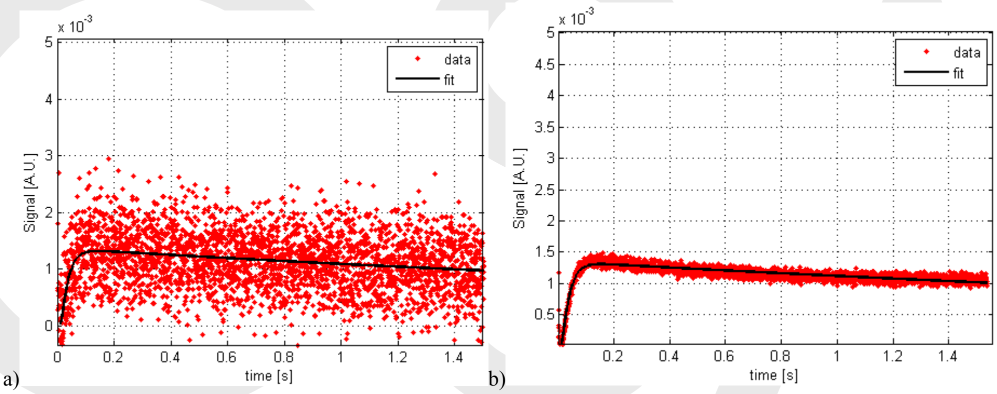

Fig. 6. Results of the AISI 304 specimen measurements. Experimental data and fitting curve for a single shot (a) and for the average of 100 shots (b). The noise level is significantly lower for the average (b).

The lower noise of the averaged value improves the quality and the calculation speed of the fit. The results for Zirconium oxide are shown in Tab. 3, for the different experimental conditions.

Table 3. Results for the measurement series #2-#4 on ZrO_2. *single fit

Series and Method	Estimated parameter α/l^2 [s^{-1}]	Standard deviation of the fitting error [a.u.]	Signal-to-noise ratio [a.u.]
#2 ZrO_2 - Room temperature Fit on the average value	0.30	$1.9 \cdot 10^{-4}$	71.3
#2 ZrO_2 - Room temperature Average of the fits on each repetition	0.30	$5 \cdot 10^{-4}$*	27.1*
#3 ZrO_2 - Room temperature - Vacuum Fit on the average value	0.29	$1.2 \cdot 10^{-4}$	38.1
#3 ZrO_2 - Room temperature -	0.29	$4.8 \cdot 10^{-4}$*	9.8*

Vacuum Average of the fits on each repetition			
#4 ZrO_2 - 1100 °C Fit on the average value	0.19	$2.2 \cdot 10^{-4}$	136.6
#4 ZrO_2 - 1100 °C Average of the fits on each repetition	0.19	$6.2 \cdot 10^{-4}$*	48.3*

As expected, also in this case the estimation of the parameter is equal for the fit on the average value and for the average of the fits on each repetition. The decrease of the signal-to-noise ratio for the room temperature measurement in the vacuum case is due to the presence of the bell jar, as the infrared windows before and after the sample contribute to a decrease of the signal. For the ZrO_2 the decrease of the estimated parameter for the high temperature experiment is expected, see also [18]. Figure 7 shows, as for the AISI specimen, the improvement of the averaged measurement compared to a single one. With respect to Fig. 6, the signal is stronger due to the high temperature measurement.

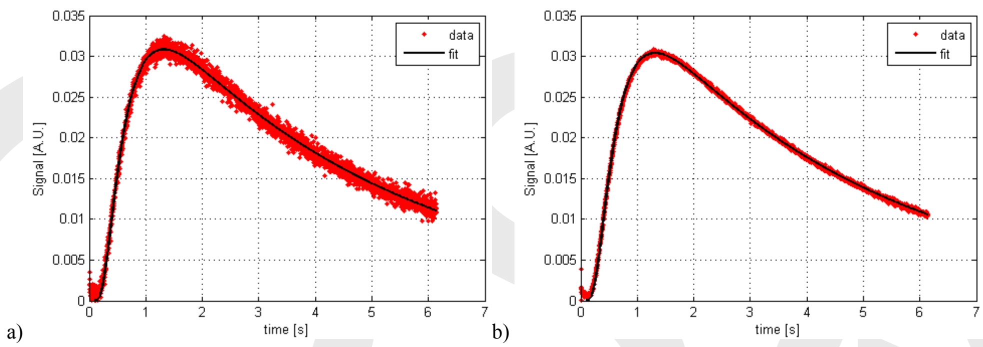

Fig. 7. Results of the ZrO_2 specimen measurements at 1100 °C. Experimental data and fitting curve for a single shot (a) and for the average of 16 shots (b). As for the AISI 304, the noise level is significantly lower for the average (b).

The experiments presented in this work have a sufficient SNR to enable the process on a single fit and have been chosen to demonstrate the equivalence of the obtained result. Working with lower laser inputs or with specimens having more challenging configurations (e.g. low thermal diffusivity or investigating thick samples) may lead to the impossibility of performing a fit on a single profile, leaving only the fit on the average profile as a feasible method

6. Conclusions

The existing laser flash setup has been improved with the creation of a software in Labview environment and the use of a new data acquisition and control board. It is now possible to repeat automatically a preselected number of measurements on a single specimen, improving significantly the signal-to-noise ratio of the measure in an easily manageable way. Results on different materials (AISI 304 and ZrO_2) and different testing conditions (room temperature, vacuum, high temperature) showed the predicted increase in SNR due to the proposed averaging method. This setup facilitates working with low laser input power and with specimens that have an unfavorable combination of thermal properties and thickness. Future work will investigate the mathematical modeling, to determine the optimal data treatment for the averaging of multiple measurements.

Disclosures

The authors declare no conflicts of interest.

References

1. S. M. Shepard, J. Hou, J. R. Lhota, and J. M. Golden, "Automated processing of thermographic derivatives for quality assurance," Opt. Eng **46**, 051008-051008–6 (2007).
2. P. Cielo, R. Lewak, and D. L. Balageas, "Thermal Sensing For Industrial Quality Control," in (1986), Vol. 0581, pp. 47–54.
3. J. D. Achenbach, "Quantitative nondestructive evaluation," International Journal of Solids and Structures **37**, 13–27 (2000).
4. V. Vavilov, "Thermal NDT: historical milestones, state-of-the-art and trends," Quantitative InfraRed Thermography Journal **11**, 66–83 (2014).
5. G. Ferrarini, P. Bison, A. Bortolin, G. Cadelano, and S. Rossi, "Thermal diffusivity measurement of ring specimens by infrared thermography," in *Thermosense: Thermal Infrared Applications Xxxix*, P. Bison and D. Burleigh, eds. (Spie-Int Soc Optical Engineering, 2017), Vol. 10214, p. UNSP 102140Z.
6. G. Ferrarini, P. Bison, A. Bortolin, and G. Cadelano, "Thermal response measurement of building insulating materials by infrared thermography," Energy and Buildings **133**, 559–564 (2016).
7. G. Cadelano, P. Bison, A. Bortolin, G. Ferrarini, F. Peron, M. Girotto, and M. Volinia, "Monitoring of historical frescoes by timed infrared imaging analysis," Opto-Electronics Review **23**, 102–108 (2015).
8. Y. Jannot and A. Degiovanni, *Thermal Properties Measurement of Materials*, Thermal Properties Measurement of Materials (2018).
9. "ASTM E1461 - 13 Standard Test Method for Thermal Diffusivity by the Flash Method," (2013).
10. W. J. Parker, R. J. Jenkins, C. P. Butler, and G. L. Abbott, "Flash Method of Determining Thermal Diffusivity, Heat Capacity, and Thermal Conductivity," Journal of Applied Physics **32**, 1679–1684 (1961).
11. P. G. Bison, S. Marinetti, A. Mazzoldi, E. Grinzato, and C. Bressan, "Cross-comparison of thermal diffusivity measurements by thermal methods," Infrared Physics & Technology **43**, 127–132 (2002).
12. I. Philippi, J. C. Batsale, D. Maillet, and A. Degiovanni, "Measurement of thermal diffusivities through processing of infrared images," Review of Scientific Instruments **66**, 182–192 (1995).
13. D. Moskal, J. Martan, V. Lang, M. Švantner, J. Skála, and J. Tesař, "Theory and verification of a method for parameter-free laser-flash diffusivity measurement of a single-side object," International Journal of Heat and Mass Transfer **102**, 574–584 (2016).
14. M. Rides, J. Morikawa, L. Halldahl, B. Hay, H. Lobo, A. Dawson, and C. Allen, "Intercomparison of thermal conductivity and thermal diffusivity methods for plastics," Polymer Testing **28**, 480–489 (2009).

15. F. Cernuschi, I. O. Golosnoy, P. Bison, A. Moscatelli, R. Vassen, H.-P. Bossmann, and S. Capelli, "Microstructural characterization of porous thermal barrier coatings by IR gas porosimetry and sintering forecasts," Acta Materialia **61**, 248–262 (2013).
16. F. Cernuschi, P. Bison, D. E. Mack, M. Merlini, S. Boldrini, S. Marchionna, S. Capelli, S. Concari, A. Famengo, A. Moscatelli, and W. Stamm, "Thermo-physical properties of as deposited and aged thermal barrier coatings (TBC) for gas turbines: State-of-the art and advanced TBCs," Journal of the European Ceramic Society **38**, 3945–3961 (2018).
17. F. Cernuschi and P. Bison, "The Influence of the Laser Energy on the Thermal Diffusivity Evaluation of TBC by Laser Flash," J Therm Spray Tech **17**, 465–472 (2008).
18. R. E. Taylor, "Thermal conductivity determinations of thermal barrier coatings," Materials Science and Engineering A **245**, 160–167 (1998).
19. J. Blumm and J. Opfermann, "Improvement of the mathematical modeling of flash measurements," High Temperatures-High Pressures **34**, 515–521 (2002).
20. T. Baba and A. Ono, "Improvement of the laser flash method to reduce uncertainty in thermal diffusivity measurements," Meas. Sci. Technol. **12**, 2046 (2001).
21. M. Akoshima and T. Baba, "Study on a Thermal-diffusivity Standard for Laser Flash Method Measurements," Int J Thermophys **27**, 1189–1203 (2006).
22. L. Vozár and W. Hohenauer, "Measurement of the thermal diffusivity by the laser-flash method with repeated pulses," High Temperatures - High Pressures **33**, 9–16 (2001).
23. E. Ruffio, C. Pradere, A. Sommier, J.-C. Batsale, A. Kusiak, and J.-L. Battaglia, "Signal noise ratio improvement technique for bulk thermal diffusivity measurement," International Journal of Thermal Sciences **129**, 385–395 (2018).
24. G. A. F. Seber and C. J. Wild, *Nonlinear Regression* (John Wiley & Sons, 1989).